J Neurophysiol 106: 1954–1968, 2011.
First published July 20, 2011; doi:10.1152/jn.00116.2011.

Coding movement direction by burst firing in electrosensory neurons

Navid Khosravi-Hashemi,[1,2] Eric S. Fortune,[3,4] and Maurice J. Chacron[1,2]

[1]*Department of Physiology and* [2]*Center for Applied Mathematics in Biology and Medicine, McGill University, Montreal, Quebec, Canada; and* [3]*Department of Psychological and Brain Sciences and* [4]*Department of Neuroscience, Johns Hopkins University, Baltimore, Maryland*

Submitted 9 February 2011; accepted in final form 17 July 2011

Khosravi-Hashemi N, Fortune ES, Chacron MJ. Coding movement direction by burst firing in electrosensory neurons. *J Neurophysiol* 106: 1954–1968, 2011. First published July 20, 2011; doi:10.1152/jn.00116.2011.—Directional selectivity, in which neurons respond strongly to an object moving in a given direction ("preferred") but respond weakly or not at all to an object moving in the opposite direction ("null"), is a critical computation achieved in brain circuits. Previous measures of direction selectivity have compared the numbers of action potentials elicited by each direction of movement, but most sensory neurons display patterning, such as bursting, in their spike trains. To examine the contribution of patterned responses to direction selectivity, we recorded from midbrain neurons in weakly electric fish and found that most neurons responded with a combination of both bursts and isolated spikes to moving object stimuli. In these neurons, we separated bursts and isolated spikes using an interspike interval (ISI) threshold. The directional bias of bursts was significantly higher than that of either the full spike train or the isolated spike train. To examine the encoding and decoding of bursts, we built biologically plausible models that examine *1*) the upstream mechanisms that generate these spiking patterns and *2*) downstream decoders of bursts. Our model of upstream mechanisms uses an interaction between afferent input and subthreshold calcium channels to give rise to burst firing that occurs preferentially for one direction of movement. We tested this model in vivo by application of calcium antagonists, which reduced burst firing and eliminated the differences in direction selectivity between bursts, isolated spikes, and the full spike train. Our model of downstream decoders used strong synaptic facilitation to achieve qualitatively similar results to those obtained using the ISI threshold criterion. This model shows that direction selective information carried by bursts can be decoded by downstream neurons using biophysically plausible mechanisms.

direction selectivity; neural coding; weakly electric fish; action potential patterning

DIRECTIONAL SELECTIVITY, in which neurons respond selectively to a given direction of movement over the opposite direction, is perhaps the most widely known computation performed by sensory neurons and is a correlate of movement perception (Hubel and Wiesel 1962). Several models have been proposed to explain how directional selectivity arises (Borst 2007; Derrington et al. 2004; Hock et al. 2009; Maex and Orban 1991). In particular, the Reichardt model for generating directionally selective responses to moving objects requires at least two fundamental operations (Reichardt 1987; Reichardt and Wenking 1969): asymmetric filtering of information from at least two spatial locations within the receptive field and nonlinear integration of these inputs. These so-called "Reichardt detectors" have received considerable attention and have been described in neural circuits across animal species (Borst and Egelhaaf 1989, 1990; Chacron and Fortune 2010; Chacron et al. 2009; Euler et al. 2002; Haag et al. 2004; Hubel and Wiesel 1962; Jagadeesh et al. 1997; Priebe and Ferster 2008; Priebe et al. 2004; Srinivasan et al. 1999).

Directional selectivity has been traditionally characterized by considering the spike train as a whole. Previously used measures of direction selectivity compare the numbers of action potentials elicited by each direction of stimulus movement. However, most vertebrate sensory neurons display distinctive patterning in their spike trains, such as the production of bursts of spikes (i.e., the firing of packets of action potentials followed by quiescence) (Gray and Singer 1989; Krahe and Gabbiani 2004; Lisman 1997; Macleod and Laurent 1996; Sherman 2001; Sherman and Guillery 2006; Sillito et al. 1994). These patterns can arise from many biophysical sources, including a variety of voltage-gated conductances. For example, subthreshold T-type calcium channels, which can act as the necessary nonlinear integrator for generating directionally selective responses in weakly electric fish (Chacron and Fortune 2010), can also give rise to burst firing (Llinas and Jahnsen 1982; Sherman 2001; Sherman and Guillery 2002, 2006).

Burst firing is ubiquitous in the central nervous system (CNS) circuits (Krahe and Gabbiani 2004) and may serve multiple functions, including feature detection (Chacron and Bastian 2008; Chacron et al. 2001, 2004; Deemyad et al. 2011; Gabbiani et al. 1996; Kepecs and Lisman 2003; Lesica and Stanley 2004; Martinez-Conde et al. 2002; Oswald et al. 2004; Sherman 2001), coding for stimulus attributes such as intensity and slope (Avila-Akerberg and Chacron 2011; Avila-Akerberg et al. 2010; DeBusk et al. 1997; Eyherabide et al. 2008; Gaudry and Reinagel 2008; Kepecs et al. 2002; Marsat and Pollack 2010; Martinez-Conde et al. 2002; Oswald et al. 2007; Samengo and Montemurro 2010), and improving the reliability of synaptic transmission (Lisman 1997; Reinagel et al. 1999). In the present study we investigated the coding of movement direction by bursts and isolated spikes (i.e., the spikes that are not part of bursts) in sensory neurons.

We used a well-suited model system, weakly electric fish, which sense distortions of their self-generated electric organ discharge (EOD) through an array of electroreceptor neurons on their skin (Chacron et al. 2011; Fortune and Chacron 2011; Turner et al. 1999). These electroreceptors project onto pyramidal cells within the hindbrain, which in turn project onto neurons within the midbrain torus semicircularis (TS). The TS is homologous to the mammalian inferior colliculus. Although previous studies have shown that TS neurons display directional selectivity to moving objects (Chacron and Fortune

Address for reprint requests and other correspondence: M. J. Chacron, 3655 Sir William Osler, Rm. 1137, Montreal, QC, Canada H3G 1Y6 (e-mail: maurice.chacron@mcgill.ca).

2010; Chacron et al. 2009, 2011), these measurements were made by considering all of the action potentials in the spike train or the membrane potential and thus did not specifically examine the contributions of action potential patterns such as bursts or isolated spikes.

METHODS

Animals. We used the weakly electric fish *Apteronotus leptorhynchus* in this study. Animals were obtained from tropical fish suppliers and were housed in laboratory tanks for several days to become acclimated to the new environment. Fish husbandry was performed according to published guidelines (Hitschfeld et al. 2009). The surgical and experimental procedures have been described in detail elsewhere (Avila-Akerberg et al. 2010; Bastian et al. 2002; Chacron 2006; Chacron and Bastian 2008; Chacron and Fortune 2010; Chacron et al. 2003, 2005a, 2007, 2009; Krahe et al. 2008; Savard et al. 2011; Toporikova and Chacron 2009). The animals were immobilized by intramuscular injection of a nicotinic receptor antagonist tubocurarine (~4 μg/g; Sigma-Aldrich, St. Louis, MO) and respirated via a mouth tube with aerated tank water at a flow rate of ~10 ml/min. The fish was submerged in water except for the top of its head. To expose the midbrain for recording, we first locally anesthetized the skin on the skull by applying 2% lidocaine. We then removed ~6 mm^2 of skin to expose the skull, to which a metal post was glued for stabilization. We drilled a hole of ~2 mm^2 in the skull above the midbrain. The surface of the brain was covered by saline throughout the experiment. All experimental procedures and animal husbandry followed guidelines established by the National Research Council and the Society for Neuroscience and were approved by the Institutional Animal Care and Use Committees of the Marine Biological Laboratory, McGill University, and the Johns Hopkins University.

Stimulation and recording. Recordings from TS neurons were made using previously described techniques (Chacron and Fortune 2010; Chacron et al. 2009; Rose and Fortune 1996). These consisted of both intracellular and extracellular recordings. Intracellular recordings and some extracellular recordings were made with patch pipettes as described previously (Rose and Fortune 1996). Other extracellular recordings were made with metal-filled micropipettes that were plated with gold and platinum at the tip (Frank and Becker 1964). Since no quantitative differences were seen when our intracellular and extracellular data set or when our extracellular data set obtained with patch pipettes was compared with our extracellular data set obtained with metal-filled micropipettes, all three data sets were pooled.

The moving stimulus consisted of a 1.8-cm-wide metal plate coated with plastic on the side opposite to the animal that was actuated using a pen plotter (HP 7010B). This object was moved back and forth along the animal's rostrocaudal axis over a distance of 20 cm (Chacron and Fortune 2010; Chacron et al. 2009; Ramcharitar et al. 2005, 2006) for at least 30 cycles (Fig. 1*A*). The sinusoid was centered at the animal's midpoint and had a frequency of 0.25 Hz (i.e., a cycle duration of 4 s), corresponding to an average velocity of ~10 cm/s. These velocities are similar to those that the animal experiences during prey capture (Nelson and MacIver 1999) and furthermore are within the range of velocities seen during refuge tracking (Cowan and Fortune 2007).

To determine whether midbrain neurons were responsive to information from tuberous electroreceptors, we also delivered amplitude modulations of the animal's own EOD that were applied via chloridized silver wire electrodes positioned 19 cm away from the fish on either side of the animal (Toporikova and Chacron 2009). Such stimuli selectively activate the tuberous but not the ampullary system (Bastian et al. 2002). The zero crossings of the amplified EOD signal (DAM50; World Precision Instruments, Sarasota, FL; band-pass filter between 300 Hz and 3 kHz) were detected by a window discriminator, which then triggered a function generator to output a single-cycle sinusoid of slightly higher frequency than the fish's EOD. This created a train of single-cycle sinusoids that were phase-locked to the EOD. The train was then multiplied (MT3 multiplier; Tucker Davis Technologies, Gainesville, FL) with a modulation waveform produced by a Power1401 (Cambridge Electronic Design, Cambridge, UK). The resulting signal was attenuated (LAT45 attenuator; Leader Electronics, Cypress, CA) and fed into the tank via a stimulus isolator (A395 linear stimulus isolator; World Precision Instruments). Depending on the polarity of the signal relative to the fish's EOD, the signal led to an increase or a decrease in amplitude of the EOD. All TS neurons in this study responded to at least one amplitude modulation (AM) stimulus within a set of sinewaves with frequencies of 1, 2, 4, 8, 16, 32, 64, and 128 Hz and thus received tuberous input (data not shown). We did not explicitly test whether these neurons also received ampullary input.

Data were acquired with Cambridge Electronic Design Power1401 hardware and Spike2 software (Cambridge, UK) and were analyzed using Spike2 (CED) and custom-made routines in MATLAB (The Mathworks, Natick, MA). An amplitude threshold was used to obtain the action potential times from the high-pass filtered (400-Hz cutoff) recorded signal (i.e., the action potential times were taken as the times at which the signal crossed the threshold from below). We excluded neurons that had total spike counts of $<$400 spikes over the stimulus duration (typically 120 s). For a stimulus whose duration is equal to 120 s, this corresponds to keeping neurons whose firing rates were $>$3.33 Hz.

Burst classification. We used an interspike interval (ISI) threshold to separate the recorded spike trains into burst and isolated spikes (Fig. 1*B*) (Avila-Akerberg and Chacron 2011; Avila-Akerberg et al. 2010; Chacron and Bastian 2008; Deemyad et al. 2011; Kepecs and Lisman 2003; Oswald et al. 2004). Specifically, two consecutive action potentials that were separated by a time interval less than the threshold were considered as part of a burst. Spikes that were not part of bursts were included in the isolated spike train. As done previously, the burst threshold was computed as the time at which the falling phase of initial peak of the autocorrelogram crossed the 99.9% Poisson confidence limit (Fig. 1*C*) (Avila-Akerberg and Chacron 2011; Avila-Akerberg et al. 2010; Bastian and Nguyenkim 2001; Chacron and Bastian 2008). Neurons with burst or isolated spike counts $<$100 were excluded from the data pool (note that this corresponds to neurons whose burst or isolated spike event rates were $<$0.83 Hz for a stimulus duration of 120 s). This method is effective for separating bursts and isolated spikes but is acausal in nature, because one needs to know when the next spike time t_{i+1} will occur in the future to assign a spike occurring at time t_i as being part of a burst or not. Assigning spikes as being part of a burst or not on the basis of an ISI threshold thus cannot be implemented in a biologically plausible neural circuit.

Membrane potential responses to moving objects. For some neurons that were recorded from intracellularly, we plotted the average membrane potential waveform in response to the moving object and low-pass filtered (160-Hz cutoff, FIR filter in Spike2) the resulting trace to remove the action potentials. The membrane hyperpolarizations were quantified by computing the area between the membrane potential curve and its average value for which the membrane potential was less than average before the peak depolarization in each movement direction. The average was computed as the average membrane potential during a full cycle of movement.

Quantifying directional selectivity. The full spike train, the burst train (i.e., the train of spikes that belong to bursts), and the isolated spike train (i.e., the train of spikes that are isolated) were used to generate peristimulus time histograms (PSTHs) in response to the moving object. For each neuron, the preferred direction was taken as the direction of movement for which the peak firing rate was highest for the full spike train, and the other direction was termed null. We then computed a measure of directional bias (DB) as

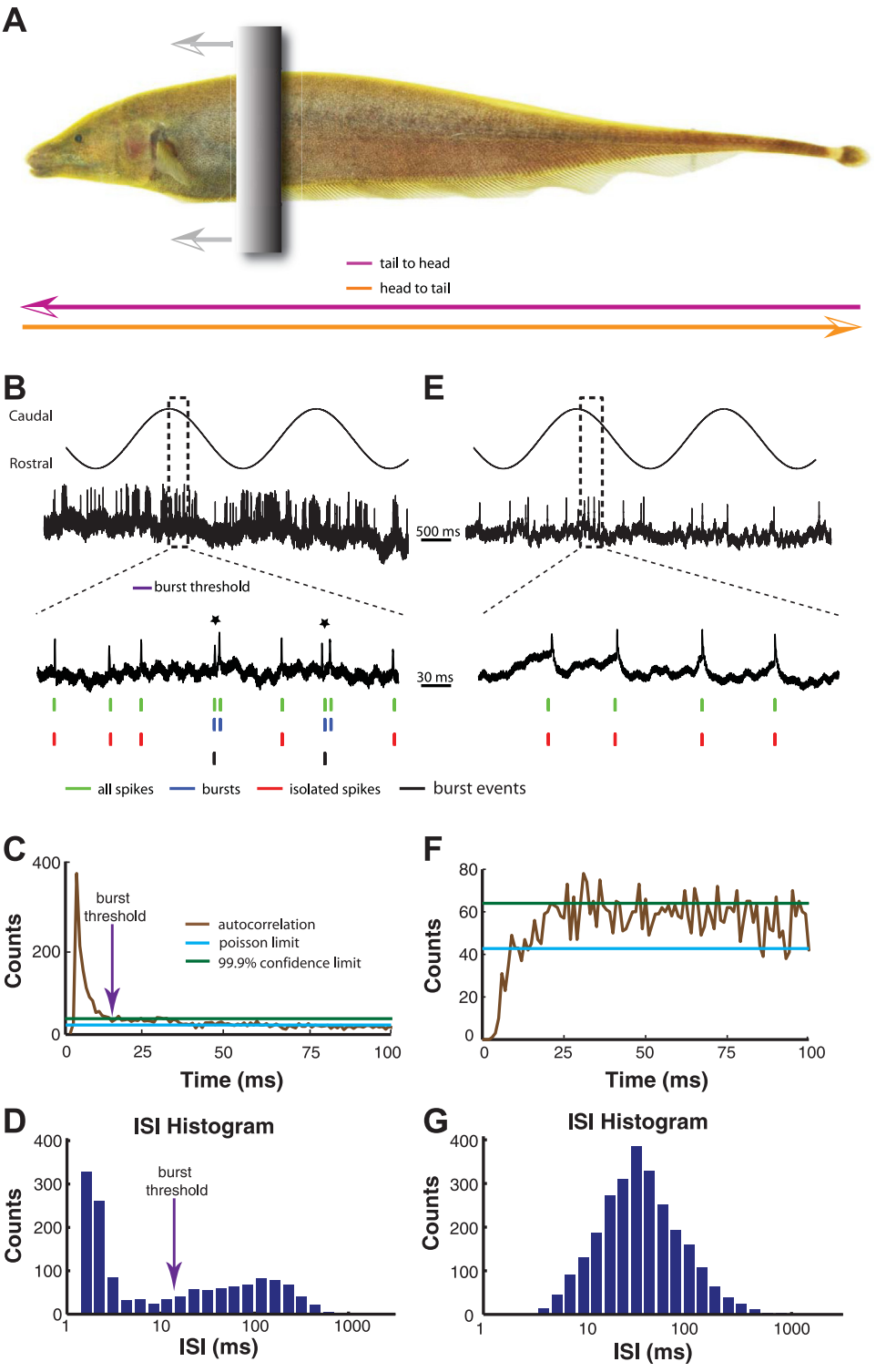

Fig. 1. Torus semicircularis (TS) neurons respond to a moving object with a combination of bursts and isolated spikes. *A*: schematic showing the stimulation protocol. The gray bar represents the moving object that was moved sinusoidally about 1 cm lateral to the fish. The purple arrow indicates the tail-to-head direction, whereas the orange arrow indicates the head-to-tail direction. *B*: example recording from a bursting TS neuron in vivo (*top*). Action potentials with interspike intervals (ISIs) that were less than the burst threshold were identified as belonging to bursts (blue ticks), whereas those that do not were identified as isolated spikes (red ticks). The set of first spike of each burst was identified as the burst event train (black ticks). *C*: spike train autocorrelogram from this same neuron. The initial peak in the autocorrelogram (brown line) is indicative of burst firing. The time lag for which the autocorrelogram falls down the 99.9% confidence interval (green line) of the expected bin contents assuming a Poisson spike train with the same mean firing rate (blue line) was chosen as the burst threshold. *D*: bimodal ISI histogram from this same neuron. The burst threshold derived from the autocorrelation function is located approximately at the trough between the 2 peaks (purple arrow). *E*: example recording from another TS neuron in vivo. In contrast, this neuron tended to fire isolated action potentials. *F*: the spike train autocorrelogram from this same neuron did not display a prominent peak and instead tended toward that of a Poisson process with the same firing rate. *G*: unimodal ISI histogram from this same neuron.

$$\mathrm{DB} = \frac{R_P - R_N}{\max(R_P, R_N)}$$

where R_P and R_N are the maximum firing rates obtained in the preferred and null directions, respectively (Chacron and Fortune 2010; Chacron et al. 2009). This measure ranges between 0 (no directional selectivity) and 1 (complete directional selectivity).

Pharmacology. As done previously, we used pressure to inject mibefradil (1 mM; Sigma-Aldrich), $NiCl_2$ (1 mM; Sigma-Aldrich), and artificial cerebrospinal fluid (ACSF) into the brain (Chacron and Fortune 2010). $NiCl_2$ is a broad-spectrum calcium channel antagonist, whereas mibefradil is selective for T-type calcium channels at the concentration used in this study (Bloodgood and Sabatini 2007; Chacron and Fortune 2010; Mehrke et al. 1994). A patch pipette with a large tip diameter (~0.5 mm) was connected to a 50-ml syringe and advanced into the TS close to the recording pipette. Gentle pressure was then applied to the syringe to eject the drug without disrupting the intracellular recording. Directional selectivity and burst firing were compared in neurons recorded under control conditions and after the injection of $NiCl_2$, mibefradil, and ACSF. Both $NiCl_2$ and mibefradil

were effective for at least 3 h after injection (Chacron and Fortune 2010). Because both $NiCl_2$ and Mibefradil had quantitatively similar effects on directional selectivity and burst firing, the data were pooled.

Modeling TS neurons. A TS neuron's receptive field was modeled in one dimension by two contiguous zones of length $d = 10$ mm each. A point object was then moved back and forth across the receptive field at a speed of 10 cm/s. The outputs $O(t)$ of each zone i are then given by

$$O_i(t) = F_i + G_i\Theta(t - \lambda_i)\exp\left(-\frac{t}{\tau_i}\right)$$

where G_i and τ_i are, respectively, the gain and depression time constant associated with zone i and λ_i is the time at which the object first enters zone i (i = ON or OFF). The ON zone represents the output of E-type electrosensory lateral line lobe (ELL) pyramidal cells that are excited by the moving object, whereas the OFF zone represents the output of I-type ELL pyramidal cells that are inhibited by the moving object (Saunders and Bastian 1984). The term F_i is a bias that represents the known baseline activity from these cells, which are approximately equal, on average (Chacron et al. 2005b; Krahe et al. 2008). We further note that the contiguous ON and OFF zones are consistent with the receptive field structure of some TS neurons (see Fig. 4*B* of Chacron et al. 2009). The input $I(t)$ to our neuron model is given by

$$I(t) = O_{ON}(t) + O_{OFF}(t)$$

Both zones project onto our model TS neuron in an excitatory fashion consistent with known anatomical data (Carr and Maler 1985). I(t) was then convolved with an alpha function with a time constant of 20 ms to mimic excitatory postsynaptic potentials (EPSPs) to obtain the input $I_c(t)$. The TS neuron was modeled using the Hodgkin-Huxley formalism. We included leak, spiking sodium, delayed rectifier potassium, and low-threshold calcium (T-type) conductances based on available experimental data (Chacron and Fortune 2010). The model is described by the following equations:

$$C\frac{dV}{dt} = -g_{leak}(V - E_{leak}) - g_T s_\infty^3 h(V - E_{Ca}) - g_{Na} m_\infty^3(V)(0.85 - n)(V - E_{Na}) - g_k n^4(V - E_K) + AI_c(t) + I_{bias} + \sigma\xi(t)$$

$$\frac{dh}{dt} = \Phi\frac{h_\infty(V) - h}{\tau_h}$$

$$\frac{dn}{dt} = \frac{n_\infty(V) - n}{\tau_n}$$

$$m_\infty(V) = \alpha_m(V)/[\alpha_m(V) + \beta_m(V)]$$

$$n_\infty(V) = \alpha_n(V)/[\alpha_n(V) + \beta_n(V)]$$

$$\tau_n(V) = 0.05/[\alpha_n(V) + \beta_n(V)]$$

$$\alpha_m(V) = 0.1(V + 40.7)/\{1 - \exp[-0.1(V + 40.7)]\}$$

$$\beta_m(V) = 4\exp[-0.05(V + 49.7)]$$

$$\alpha_n(V) = 0.01(V + 40.7)/\{1 - \exp[-0.1(V + 40.7)]\}$$

$$\beta_n(V) = 0.125\exp[-0.0125(V + 50.7)]$$

$$s_\infty(V) = \frac{1}{1 + \exp[-(V + 69)/7.8]}$$

$$h_\infty(V) = \frac{1}{0.5 + \sqrt{0.25 + \exp[(V + 82)/6.3]}}$$

where C is the membrane capacitance, V is the transmembrane potential difference, and g_{leak} is the leak conductance with reversal potential E_{leak}. In this study, g_T, g_{Na}, and g_K are the voltage-gated calcium, sodium, and potassium conductances with reversal potentials E_{Ca}, E_{Na}, and E_K, respectively. A is the synaptic weight, I_{bias} is a constant bias current, and $\sigma\xi(t)$ is zero mean low-pass filtered Gaussian white noise with standard deviation σ that mimics sources of synaptic input (Manwani and Koch 1999). These equations were previously used to model burst firing in thalamic relay neurons, and a full description of the burst mechanism in the deterministic regime (i.e., $\sigma = 0$) can be found in Rush and Rinzel (1994).

We simulated this model numerically using an Euler-Maruyama algorithm (Kloeden and Platen 1999) with integration time step dt = 0.0025 ms. Other parameter values used, unless otherwise stated, were $g_{leak} = 0.18$ μS, $\tau_h = 30$ ms, $g_T = 0.32$ μS, $g_{Na} = 30$ μS, $g_K = 10$ μS, $E_{leak} = -65$ mV, $E_{Ca} = 120$ mV, $E_{Na} = 60$ mV, $E_K = -85$ mV, $C = 1$ μF, $A = 0.75$ nA, $\Phi = 2$, $G_{ON} = 1$, $G_{OFF} = -1$, $F_{ON} = F_{OFF} = 2$, $I_{bias} = -4.3$ nA, $\tau_{ON} = 100$ ms, and $\tau_{OFF} = 10$ ms. We note that the negative value of G_{OFF} should not be taken to imply that TS neurons receive direct inhibition from ELL pyramidal neurons. Rather, it reflects the fact that I-type ELL pyramidal cells within that zone that excite TS neurons are inhibited by the moving object stimulus. These parameter values are comparable to those used in previous modeling studies (Chacron and Fortune 2010; Chacron et al. 2009; Rush and Rinzel 1994) and to the experimentally observed time constant of depression (Chacron et al. 2009). The simulated spiking responses were then used to build PSTHs over 2,000 presentations of the moving stimulus and were segregated into bursts and isolated spikes as described above using an ISI threshold of 10 ms (Oswald et al. 2004). The DB was then computed in the same way as we did for the data.

Modeling biophysically plausible mechanisms to extract bursts. Although the ISI threshold procedure described above is a simple computational method for segregating bursts from isolated spikes, the method is acausal and therefore cannot be implemented in brain circuits on a spike-by-spike fashion, because it is necessary to know when the next spike will occur to classify a spike happening at the present time as being part of a burst or not. It was previously proposed that a synapse that exhibited strong facilitation would be largely unresponsive to isolated spikes but sensitive to bursts (Kepecs and Lisman 2003; Kepecs et al. 2002; Lisman 1997). We thus considered such a circuit, using well-established techniques to model and quantify short-term synaptic plasticity (Dayan and Abbott 2001; Gabbiani and Koch 1998; Rieke et al. 1996). Specifically, we considered the presynaptic spike train as a sum of delta functions:

$$X(t) = \sum_{i=1}^{N}\delta(t - t_i)$$

where t_i is the ith spike time. The amplitude of the synaptic EPSP caused by the ith spike time is given by the product of a facilitation term, F(t_i), and a depression term, D(t_i), that obey the following dynamics (Harvey-Girard et al. 2010; Lewis and Maler 2002, 2004; Lindner et al. 2009):

$$\frac{dD}{dt} = \frac{1 - D}{\tau_d};\ t = t_i \Rightarrow D(t_i) \rightarrow D(t_i)[1 - F(t_i)]$$

$$\frac{dF}{dt} = \frac{F}{\tau_f};\ t = t_i \Rightarrow F(t_i) \rightarrow F(t_i) + \Delta F(t_i - t_{i-1})$$

$$\Delta F(I) = \frac{I_0}{I}$$

At the time of an input spike t_i, D is first decreased by an amount F(t_i)D(t_i); F is then updated by an increment ΔF. The increment ΔF is inversely proportional to the time interval between the current action potential and the last one. Short time intervals such as those that occur during burst firing will cause more potentiation than longer ones. We have also introduced an upper bound for F [i.e., F(t) $\leq$ 1] to prevent negative values for the update factor of the depression variable. We

used a Euler algorithm to simulate this model with an integration time step of 0.025 ms. The output of the model was convolved with an alpha function with the time constant $\tau_\alpha = 4$ ms to mimic synaptic PSPs. Thus the output is given by

$$Y(t) = \sum_{i=1}^{N} \Theta(t - t_i)\mathrm{D}(t_i)\mathrm{F}(t_i)\frac{t - t_i}{\tau_\alpha^2}\exp\left(-\frac{t - t_i}{\tau_\alpha}\right)$$

where $\Theta(t)$ is the Heaviside function [$\Theta(t) = 1$ if $t \geq 0$ and $\Theta(t) = 0$ otherwise]. Other parameter values used were facilitation time constant $\tau_f = 70$ ms and depression time constant $\tau_d = 500$ ms. The transfer function (TF) of the postsynaptic neuron is given by the following:

$$\mathrm{TF}(Y) = \begin{cases} Y & \text{if} \quad Y \geq 0 \\ 0 & \text{if} \quad Y < 0 \end{cases}$$

Thus the output of the postsynaptic neuron is given by

$$Z(t) = \mathrm{TF}[Y(t)]$$

We then took experimentally recorded spike sequences and segregated them into bursts and isolated spikes using both our decoding model and ISI threshold methods. We then compared the sequences of burst and isolated spikes obtained from each model in the following way. We used signal detection theory (Green and Swets 1966) to quantify the decoding model's performance at detecting bursts as defined by the ISI threshold. We computed the probability of correct detection (P_D) as the fraction of spike times deemed to be part of a burst according to the decoding model that were also deemed part of a burst using the ISI threshold criterion (i.e., that were "correctly" classified). The probability of false alarm (P_{FA}) was computed as the fraction of spike times deemed to be part of a burst according to the decoding model that were deemed to be isolated using the ISI threshold criterion (i.e., that were "incorrectly" classified). The overall performance can then be quantified by computing the probability of correct classification (P_{cc}) as

$$P_{cc} = \frac{P_D}{2} + \frac{(1 - P_{FA})}{2}$$

A value of $P_{cc} = 0.5$ implies that our model performs at chance level compared with the ISI threshold criterion (i.e., that any given spike is randomly assigned as being part of a burst or isolated). In contrast, $P_{cc} = 1$ indicates that the model performs identically to the ISI threshold criterion. We note that this does not imply that the ISI threshold criterion is optimal in any way at segregating bursts and isolated spikes, merely that our biophysically plausible decoding model performs as well. We used signal detection theory to determine how well the decoding model performs relative to the ISI threshold criterion. To investigate the robustness of the model's performance, we computed the probability of correct classification of bursts over a wide range of physiologically plausible τ_f and τ_d time constants.

RESULTS

Bursts preferentially code for movement direction in TS neurons. We performed in vivo extracellular recordings from TS neurons ($n = 43$) while moving an object back and forth along the rostrocaudal axis of the animal (Fig. 1*A*). We found that most neurons ($n = 36$, or ~70%) fired bursts of action potentials in response to the moving object (Fig. 1*B*). This firing pattern was reflected in a large peak in the autocorrelogram (Fig. 1*C*, brown line) that exceeded the 99.9% confidence interval (Fig. 1*C*, green line) around the autocorrelogram from a Poisson process with the same firing rate (Fig. 1*C*, cyan line). Such a peak has been taken to be a sign of burst firing (Abeles 1982; Bastian and Nguyenkim 2001). We used an ISI threshold criterion to separate the train of action potentials into bursts and isolated spikes (Fig. 1*B*). Specifically, when the difference between the times of two consecutive spikes was less than the threshold, the two spikes were labeled burst spikes (Kepecs and Lisman 2003; Lesica and Stanley 2004; Oswald et al. 2004). The remaining spikes were labeled isolated spikes (Fig. 1*B*).

This criterion was used to separate the spike train into the burst spike train (i.e., the train of action potentials that belong to bursts) and the isolated spike train (i.e., the train of action potentials that do not belong to bursts). The burst event train was defined as the train of action potentials that consisted of only the first spike within each burst (Oswald et al. 2004). As in previous studies, we chose the burst threshold to be equal to the time at which the autocorrelation function first crosses the 99.9% confidence interval from above (Fig. 1*C*) (Avila-Akerberg et al. 2010; Bastian and Nguyenkim 2001; Chacron and Bastian 2008). This value also corresponds to the trough in the bimodal ISI distribution from this neuron (Fig. 1*D*), which is frequently taken as the threshold to segregate bursts and isolated spikes (Deemyad et al. 2011; Doiron et al. 2003; Turner et al. 1994).

The remainder of neurons in our data set ($n = 16$, or ~30%) did not preferentially produce bursts but approached a Poisson distribution (Fig. 1*E*). The autocorrelogram (Fig. 1*F*, brown line) did not display a large peak, as shown in bursting neurons, and instead slowly rose toward the value computed from a Poisson process with the same firing rate (Fig. 1*F*, cyan line). Furthermore, the ISI distributions of these neurons were unimodal in nature (Fig. 1*G*), which indicates their tendency to not fire bursts of action potentials (Doiron et al. 2003).

Approximately 50% of directionally selective TS neurons have the tail-to-head direction as their preferred direction, whereas the other 50% have the head-to-tail direction as their preferred direction when the full spike train is considered (Chacron et al. 2009). The data obtained from a representative bursting neuron are shown in Fig. 2*A*. This neuron responded best when the object was moving from tail to head (preferred direction) and displayed a weaker response when the object was moving from head to tail (null direction) (Fig. 2, *A* and *B*). We quantified this difference using a directional bias index and found that this neuron displayed strong directional selectivity (DB = 0.62; DB = 0 indicates no directional selectivity and DB = 1 indicates complete directional selectivity).

For bursting neurons, we observed a qualitatively different sensitivity to movement direction when considering either the burst spike train (i.e., only the spikes belonging to bursts) or the isolated spike train. We found that burst spikes almost exclusively occurred when the object was moving in the preferred direction (Fig. 2, *A*, arrows, and *B*), thereby giving the burst spike train a larger directional bias (DB = 0.91) than the full spike train. Similar results were seen when considering the burst event train (DB = 0.91) (Fig. 2, *A*, arrows, and *B*). In contrast, isolated spikes were more evenly distributed (Fig. 2, *A*, arrows, and *B*) and, as a result, the isolated spike train displayed a weaker directional bias (DB = 0.33). This result is not dependent on the specific threshold for separating burst and isolated spikes: we found that the directional biases of the burst, burst event, and isolated spike trains were largely unaffected by varying the burst threshold over a wide range of values (Fig. 2*C*).

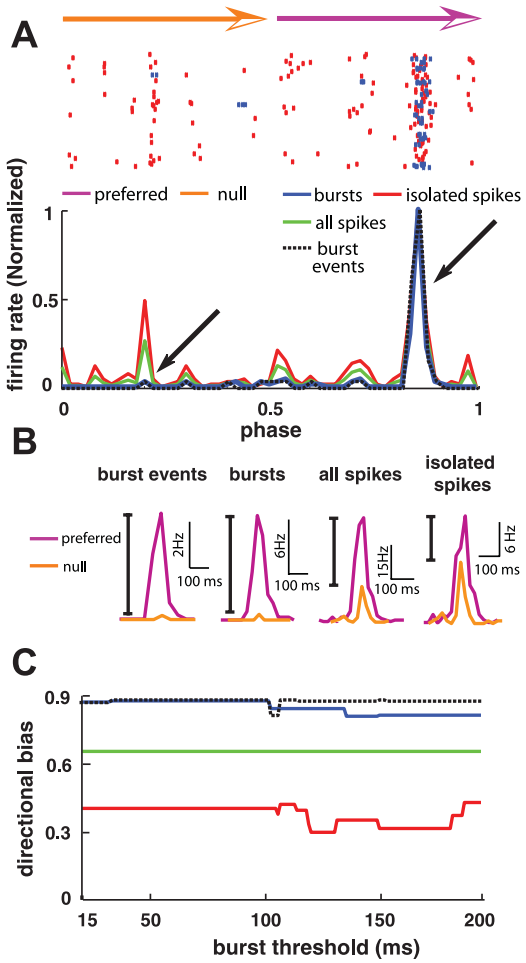

Fig. 2. Bursts carry directional information. *A*, *top*: raster plot from an example directionally selective bursting TS neuron. The spikes that belong to bursts are shown in blue, whereas isolated spikes are shown in red. *Bottom*: peristimulus time histogram (PSTH) for this same neuron computed from all spikes (both bursts and isolated spikes, green line), bursts (blue line), burst events (dotted black line), and isolated spikes (red line). Arrows highlight similarity between measures for bursts and burst events. *B*: PSTHs from burst events, bursts, all spikes, and isolated spikes aligned with respect to the maximum event rates in the preferred (pink) and null (orange) directions. Directional bias (DB) values were 0.91, 0.91, 0.62, and 0.33 for burst events, bursts, all spikes, and isolated spikes, respectively. *C*: DB values were largely insensitive to the value of the ISI burst threshold chosen.

Bursting neurons displayed a wide range of directional biases when the full spike train was considered (0–0.79). The example neuron showed in Fig. 2 was in the upper range with a directional bias of 0.62. Despite these large heterogeneities, the directional bias of bursts was significantly higher than that of all spikes ($P = 0.006$, sign rank test, $n = 32$) across these neurons. Furthermore, the directional bias for all spikes was significantly higher than for isolated spikes ($P << 0.001$, sign rank test, $n = 32$) (Fig. 3*A*). We conclude that bursts are overall more reliable indicators of the direction of movement than either the entire spike train or the isolated spikes. Moreover, the directional bias of burst events was not significantly different from that of bursts ($P = 0.1577$, sign rank test, $n = 32$). Since burst and burst events did not display significantly different levels of directional bias across our data set, we only present results obtained with the burst train from now on.

As a methodological control, we set an arbitrary threshold of 30 ms in the subset of neurons that did not produce bursts. In these neurons, the differences between the directional biases of "bursts," all spikes, and "isolated spikes" were not significantly different (bursts-all spikes: $P = 0.1$, all spikes-isolated spikes: $P = 0.2$, bursts-isolated spikes: $P = 0.07$, sign rank tests, $n = 11$; Fig. 3*B*). The directional biases of the burst and isolated spike trains were qualitatively similar for a wide range of burst threshold values (data not shown). Moreover, the directional bias from all spikes of these neurons was not significantly different from that computed from bursting neurons ($P = 0.6557$, Wilcoxon rank sum test, df = 42). We shall return to this point in the DISCUSSION.

Mechanisms for the generation of burst and isolated spike responses to moving objects. Theoretically, direction selectivity can rely on two fundamental operations (Reichardt 1987; Reichardt and Wenking 1969). The first operation involves generating a directional bias by asymmetric filtering of information from at least two separate spatial locations within the receptive field. Many mechanisms can give rise to a directional bias, including dendritic integration (Euler et al. 2002), temporal delays (Haag et al. 2004; Jagadeesh et al. 1997), and synaptic depression (Carver et al. 2008; Chacron et al. 2009; Chance et al. 1998). The second operation involves the nonlinear interaction of these inputs, and various types of nonlinearities have been considered such as multiplication (Haag et al. 2004; Reichardt 1987), squaring (Adelson and Bergen 1985), nonlinear synaptic integration (Chacron and Fortune 2010), shunting (Euler et al. 2002), and thresholding (Priebe and Ferster 2008; Priebe et al. 2004).

In TS neurons, asymmetric filtering by different time constants of synaptic depression across the receptive field creates

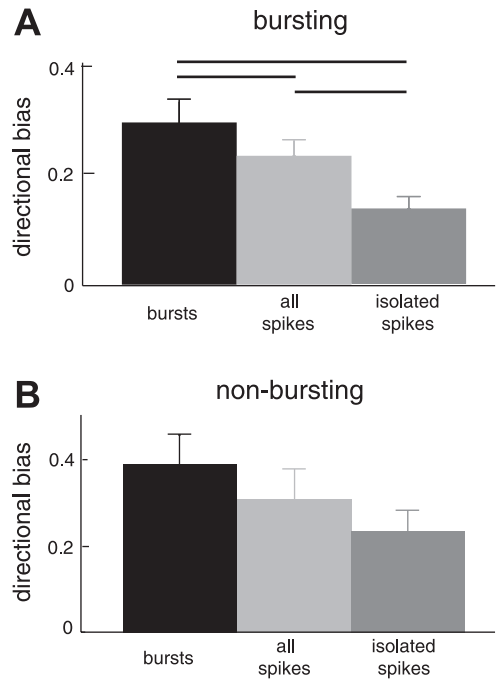

Fig. 3. Summary of directional biases obtained for bursts, all spikes, and isolated spikes for bursting and nonbursting neurons. Population-averaged DB values for bursts (black), all spikes (light gray), and isolated spikes (dark gray) are shown for bursting (A) and nonbursting (*B*) neurons. Horizontal bars indicate statistical significance at the $P = 0.05$ level using a signed-rank test.

a directional bias (Chacron et al. 2009), and these inputs are nonlinearly integrated by a subthreshold T-type conductance (Chacron and Fortune 2010). Since T-type calcium channels have been shown to give rise to burst firing in other systems (Llinas and Jahnsen 1982; Sherman 2001; Sherman and Guillery 2006), we hypothesize that these also might be responsible for burst firing in TS neurons. T-type calcium channels are inactivated at resting membrane potential values (approximately −60 mV) and require ~100 ms of hyperpolarization to approximately −70 mV to remove their inactivation, after which a subsequent depolarization will lead to a subthreshold calcium spike, leading to nonlinear integration of synaptic input. Bursts of sodium action potentials can occur on top of these calcium spikes (Rush and Rinzel 1994; Sherman and Guillery 2006). However, a simple depolarization from the resting potential will not lead to burst firing, because the calcium channel will still be inactivated and will instead lead to tonic firing (Sherman and Guillery 2006).

We therefore examined intracellular recordings from TS neurons and looked at whether a membrane hyperpolarization indeed preceded the peak firing response in each direction of movement. The data show that the peak responses in both the preferred and the null directions were preceded by a period of spiking silence (Fig. 4*A*). Furthermore, plots of average membrane potential waveforms also revealed, critically, that membrane hyperpolarizations were responsible for the lack of spiking activity and preceded the peak depolarizations (Fig. 4*B*). These hyperpolarizations were significantly larger in magnitude in the preferred direction (Fig. 4*C*, $P = 0.031$, sign rank test, $n = 6$). These results show that membrane hyperpolarization removes the inactivation of the T-type conductance, thereby giving rise to burst firing. The data also show that the hyperpolarizations are larger when the object moves in the preferred direction. This larger hyperpolarization would presumably more effectively remove the inactivation of the T-type conductance, thereby increasing the probability of burst firing when the object moves in the preferred direction.

Previously used models of directional selectivity in TS neurons did not incorporate spike firing (Chacron and Fortune 2010) and furthermore assumed only excitatory input from afferent neurons. These models thus cannot reproduce the experimentally observed membrane hyperpolarization that precedes the peak depolarization. We built a mathematical model that incorporates the known mechanisms that lead to directional selectivity in the electrosensory system and that gives rise to a larger membrane hyperpolarization when the object moves in the preferred direction.

There are two types of ELL pyramidal cells (Bastian et al. 2002; Maler 2009; Saunders and Bastian 1984), E and I, that correspond to the ON- and OFF-type cells seen in other systems. Whereas E-type pyramidal cells are excited by our metal moving object stimulus, I-type pyramidal cells are instead inhibited by it. The receptive field is modeled in one dimension as two contiguous zones: one represents the output of I-type ELL pyramidal cells, and the other represents the output of E-type ELL pyramidal cells, which have time constants of depression τ_{OFF} and τ_{ON}, respectively (Fig. 5*A*). Both the ON and OFF zones then make excitatory contact with our model TS neuron, which is consistent with anatomical data (Carr and Maler 1985). The summed input is then convolved with an alpha function to mimic the synaptic EPSP shape and

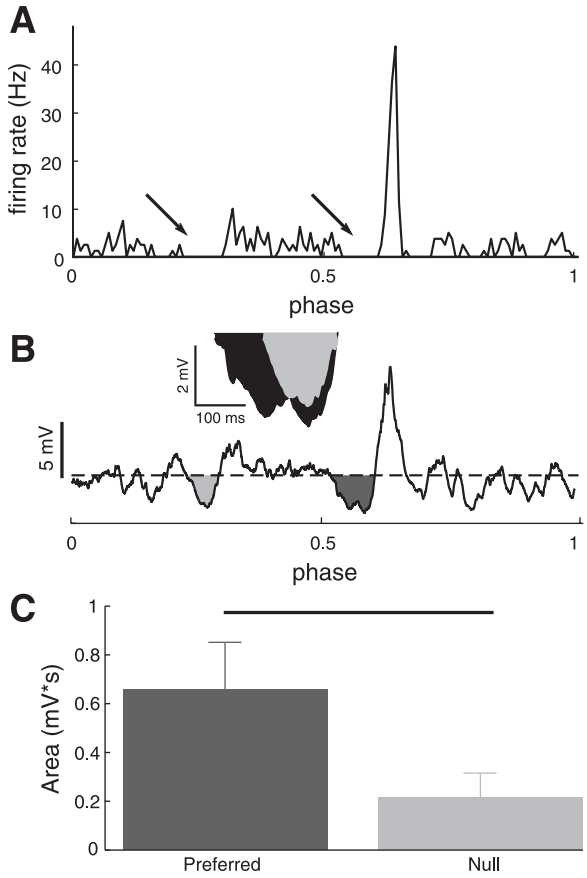

Fig. 4. A membrane hyperpolarization precedes the peak response in a directionally biased way. *A*: PSTH of an example direction-selective neuron. Periods of silence preceded the peak firing rates in both the preferred and null directions (arrows). *B*: average membrane potential waveform of the same neuron. Hyperpolarizations in the membrane potential precede the peak depolarizations in both movement directions. These hyperpolarizations are indicated with light gray shading in the null direction and dark gray shading in the preferred. Horizontal dashed line indicates the average membrane potential. The membrane hyperpolarization is stronger in the preferred direction than in the null direction (*inset*). *C*: population average of the hyperpolarization magnitude that is computed as the area for which the membrane potential is lower than average in the preferred (dark gray) and null (light gray) directions preceding the peak depolarizations ($n = 6$). The horizontal bar indicates statistical significance at the $P = 0.05$ level using a signed-rank test.

fed into a Hodgkin-Huxley model with leak, spiking sodium, delayed rectifier potassium, and T-type calcium conductances (Fig. 5*A*). It is important to note that our model considers the effects of the significant spontaneous activity of afferents that occurs in vivo (Destexhe et al. 2003) by including a noise term that induces membrane potential fluctuations. In particular, the noise term can give rise to a mixture of burst and isolated action potential firing as observed under in vivo conditions in other systems (Wolfart et al. 2005) as well as our experimental data (Fig. 1*B*).

The model stimulus was an object that moved across the receptive field in both directions. Figure 5*B* shows the responses of both the OFF and ON zones to this stimulus. When the object moves from the OFF to the ON zone, a decrease in excitation from when the object is in the OFF zone precedes an increase in excitation when the object is in the ON zone. However, when the object moves in the opposite direction, the increase in excitation is truncated by

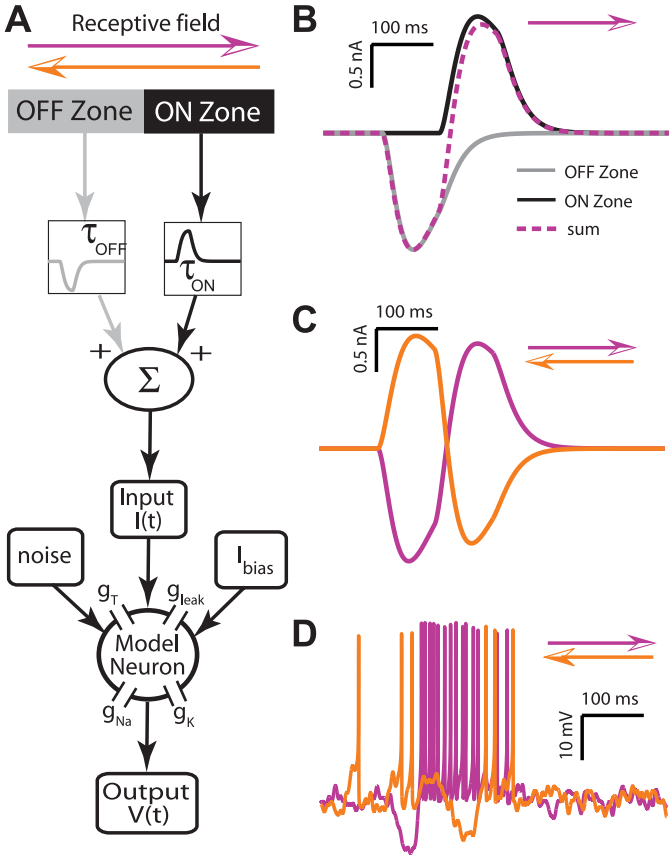

Fig. 5. Modeling directional selectivity in TS neurons. *A*: schematic of the receptive field of our model neuron that is composed of 2 zones: the OFF zone represents output from I-type ELL pyramidal cells that are inhibited by the moving object and has a synaptic depression time constant τ_{OFF}, whereas the ON zone represents output from E-type ELL pyramidal cells that are excited by the moving object and has a synaptic depression time constant τ_{ON}. The responses from each zone are then summed and convolved with an alpha function with a time constant of 20 ms and fed into a Hodgkin-Huxley model with spiking sodium (g_{Na}), delayed rectifier potassium (g_K), leak (g_{leak}), and T-type calcium (g_T) conductances. Noise and a constant bias current (I_{bias}) are also added to this model to mimic synaptic input. The output membrane potential $V(t)$ from the model is then thresholded to obtain the spike times that were analyzed in the same fashion as the experimental data. *B*: inputs from the OFF zone (gray) and ON zone (black), and the sum of both (dashed purple) for $\tau_{OFF} = \tau_{ON} = 500$ ms when the object moves from left to right (i.e., enters the OFF zone first and then enters the ON Zone). Note that the traces are aligned with respect to their baseline values to better compare their time courses. *C*: summed input when the object moves from left to right (purple, identical to trace in *B*) and when the object moves from right to left (orange). *D*: example membrane potential traces from the model responding to the inputs shown in *C*. Burst firing is dramatically increased when the object moves in the preferred direction (purple) compared with when the object moves in the null direction (orange).

the decrease in excitation (Fig. 5*C*). The membrane potential responses of the model neuron to these moving stimuli are shown in Fig. 5*D*. Interestingly, when the object moves from the OFF to the ON zone, the decrease in excitation removes the inactivation of the calcium conductance and the subsequent increase in excitation then activates it; as a result there is a strong tendency to have a calcium spike, which gives rise to a burst of action potentials (Fig. 5*D*, purple). In contrast, when the object moves from the ON zone to the OFF zone, the increase in excitation from the ON zone only gives rise to isolated spikes as the calcium conductance is then inactivated. Moreover, the weaker decrease in excitation is less effective at removing the inactivation of calcium channels. This and the fact that this decrease is not followed by an increase in excitation both contribute to our model having a lesser tendency to display burst firing in that direction (Fig. 5*D*, orange). The preferred direction is therefore when the object moves from the OFF zone to the ON zone and the null direction is the opposite direction.

Role of T-type calcium channels in generating bursts in response to moving objects. We systematically varied the T-type calcium channel conductance g_T to gauge the effects of the active burst mechanism on responses to a simulated moving object. Our results show that varying g_T can lead to qualitatively different regimes (Fig. 6*A*). As in the experimental data, we segregated bursts and isolated spikes using an ISI threshold. For lower values of g_T, bursts and isolated spikes showed similar levels of directional selectivity to all spikes (Fig. 6, *B–D*). In contrast, for higher values of g_T, bursts displayed greater directional selectivity than either all spikes or isolated spikes (Fig. 6, *E–G*). In contrast, a model that only includes ON zones but with different time constants of depression cannot reproduce this critical feature of our data (data not shown). Thus the removal of inactivation of the T-type calcium conductance by membrane hyperpolarization resulting from the decrease in excitation coming from the OFF zone is necessary for our model to reproduce the current data set.

These results show that our relatively simple mathematical model can qualitatively reproduce the experimentally observed directional biases of bursts and isolated spikes. How does this work? The inputs from the two zones for $\tau_{ON} = 100$ ms and $\tau_{OFF} = 10$ ms are shown in Fig. 7*A*. As shown above (Fig. 5*C*), a decrease in excitation is followed by an increase in excitation when the object moves in the preferred direction (Fig. 7*A*, purple). In contrast, the increase in excitation is truncated by weaker decrease in excitation when the object moves in the null direction (Fig. 7*A*, orange). As a result, for weaker values of g_T, the weaker hyperpolarization followed by no depolarization when the object moves in the null direction results in a mixture of bursts and isolated spikes (Fig. 7*B*). However, the larger hyperpolarization when the object moves in the preferred direction more effectively removes the inactivation of calcium channels, and the following depolarization elicits more action potential firing (Fig. 7*C*). However, this action potential firing still consists of bursts and isolated spikes with roughly the same proportion as when the object moves in the null direction. As such, the directional biases of bursts and isolated spikes are roughly equal.

For larger values of g_T, qualitatively different results were observed. When the object moves in the null direction, the resulting firing pattern is similar to that observed with lower values of g_T (Fig. 7*D*). In contrast, when the object moves in the preferred direction, the stronger decrease in excitation more effectively removes the inactivation of the now stronger calcium conductance, and the following depolarization now gives rise to a stronger calcium spike and thus a greater probability of obtaining burst firing and lesser probability of obtaining isolated spike firing (Fig. 7*E*). As a result, the directional bias of bursts increases while the directional bias of isolated spikes decreases with respect to their values obtained for lower g_T.

Role of T-type calcium channels in vivo. To test the model's prediction that the T-type calcium channel-mediated burst mechanism can produce bursts that display significantly more

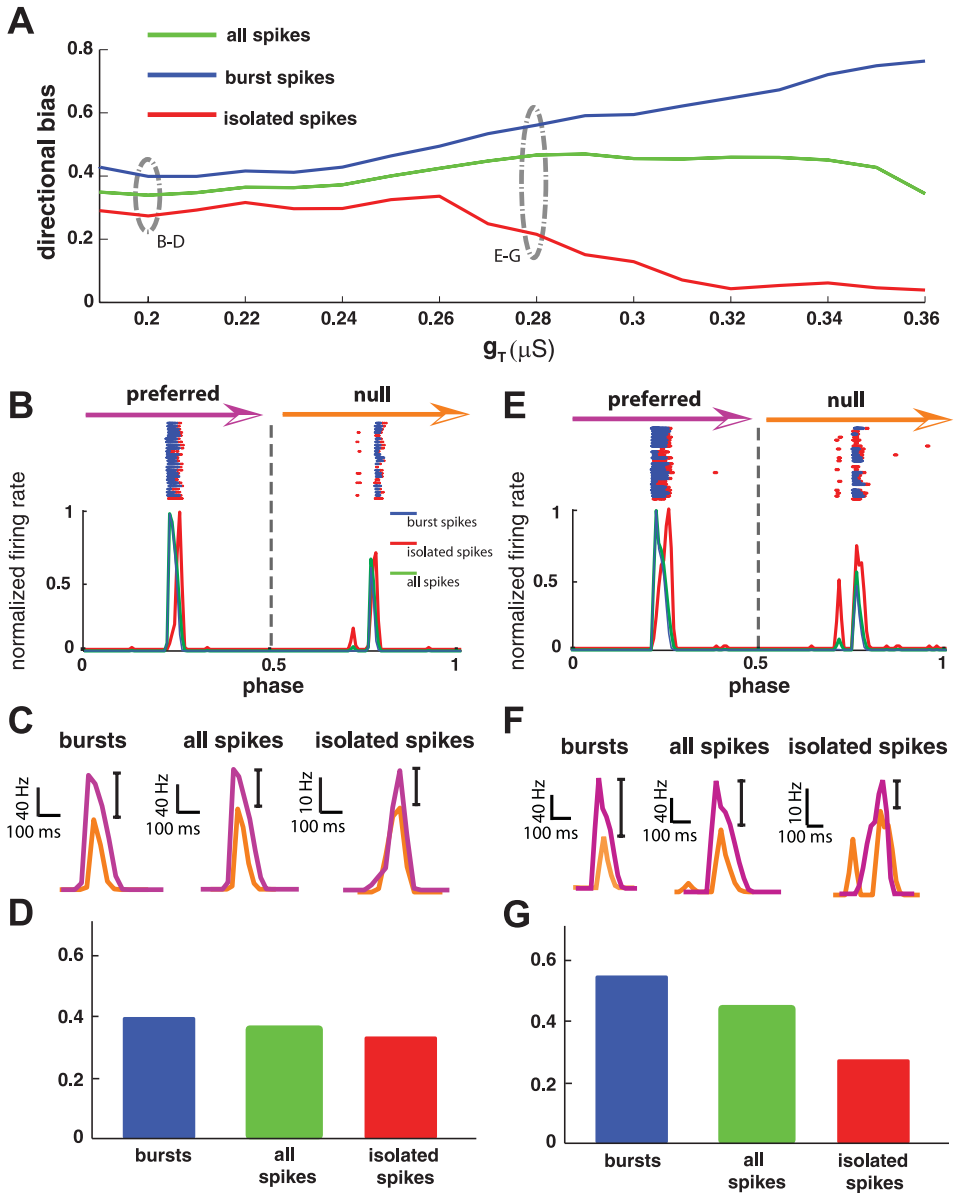

Fig. 6. Effects of burst dynamics on directional selectivity. *A*: DB values obtained from the model from all spikes (green), burst spikes (blue), and isolated spikes (red) as a function of g_T. Although bursts and isolated spikes showed similar levels of directional selectivity to all spikes for low values of g_T (*left*), a regime where bursts displayed greater DB than either all spikes or isolated spikes was observed for larger values of g_T (*right*). *B–D*: model data for $g_T = 0.2$ μS. *B*, *top*: raster plot in response to the moving object stimulus. We used an ISI threshold of 10 ms to segregate bursts (blue) from isolated spikes (red). *Bottom*: PSTH obtained from all spikes (green), bursts (blue), and isolated spikes (red). The curves have been normalized to their maximum value for easier comparisons. *C*: PSTH values near the maximum values in the preferred (purple) and null (orange) directions. *D*: DB computed from bursts (blue), all spikes (green), and isolated spikes (red) were similar. *E–G*: model data for $g_T = 0.28$ μS. *E*: raster plot (*top*) and PSTH (*bottom*) for burst spikes (blue), all spikes (green), and isolated spikes (red). *F*: PSTH values near the maximum values in the preferred (purple) and null (orange) directions. *G*: DB computed from burst spikes (blue), all spikes (green), and isolated spikes (red). Bursts displayed a greater bias than all spikes, which displayed a greater bias than isolated spikes.

directional selectivity than either all spikes or isolated spikes, we injected the antagonists $NiCl_2$ and mibefradil, as was done in previous studies (Chacron and Fortune 2010), to block the activity of T-type calcium conductances in TS neurons. Because both $NiCl_2$ and mibefradil had quantitatively similar results on directional selectivity and burst firing, the data were pooled. We found that fewer neurons displayed burst firing after injection of either $NiCl_2$ or mibefradil into the TS. In contrast, the percentage of neurons that displayed burst firing after saline injection was similar to that observed for control conditions (Fig. 8*A*).

We quantified the directional biases of bursts, isolated spikes, and all spikes before (Fig. 8*B*) and after injection of saline (Fig. 8*C*) or mibefradil and $NiCl_2$ (Fig. 8*D*). As expected, the directional bias values obtained for bursts were significantly greater than those obtained for all spikes or isolated spikes before injection (Fig. 8*B*), and injection of saline had no significant effect (compare Fig. 8*C* with Fig. 8*B*). However, after injection of $NiCl_2$ or mibefradil, the measures of direction selectivity for bursts, isolated spikes, and all spikes were dramatically altered: they were not significantly different from each other (Fig. 8*D*). Furthermore, $NiCl_2$ or mibefradil significantly reduced the directional bias of bursts ($P = 0.02$, Wilcoxon rank sum test, $n = 12$) and all spikes ($P < 0.003$, Wilcoxon rank sum test, $n = 12$), but not that of isolated spikes ($P = 0.24$, Wilcoxon rank sum test, $n = 12$), whereas saline injection did not significantly alter the directional bias of either bursts ($P = 0.51$, Wilcoxon rank sum test, $n = 12$) or isolated spikes ($P = 0.32$, Wilcoxon rank sum test, $n = 12$). These data support our modeling prediction that an active burst mechanism based on T-type calcium conductances promotes selective coding of directional information by bursts.

Mechanisms for decoding movement information from burst and isolated spike trains. Any information is only functionally relevant if it is decoded by downstream neurons. We examined biologically plausible mechanisms by which information from the burst and isolated spike trains might be discriminated in downstream decoders. This is a potentially difficult problem,

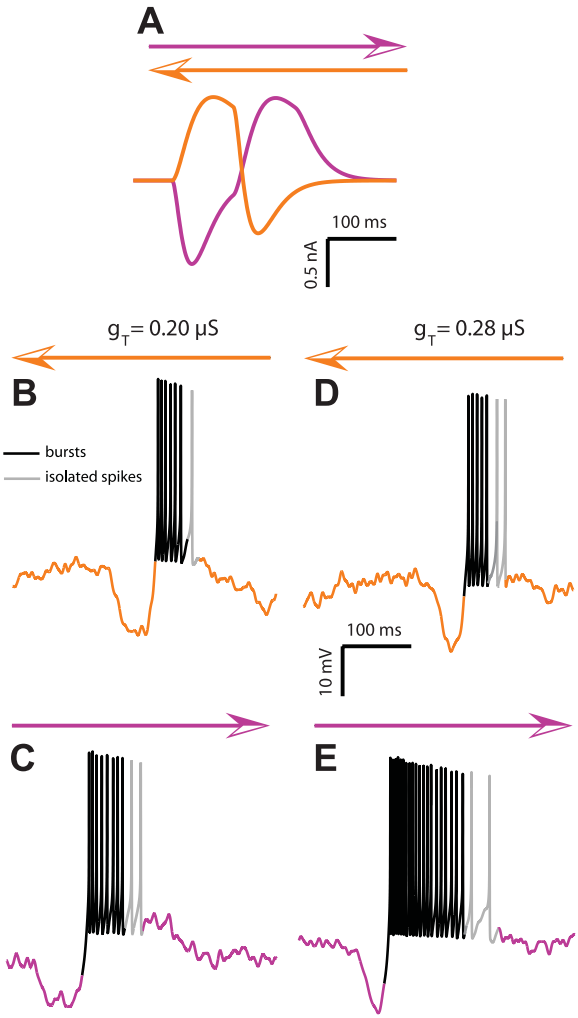

Fig. 7. Explanation of the different regimes observed in the model. *A*: summed input currents from both zones when the object moves from right to left (orange) and from left to right (purple). Example output from the model are shown with $g_T = 0.2$ μS (*B* and *C*) and with $g_T = 0.28$ μS (*D* and *E*). *B*: an example membrane potential trace when the object moves from right to left (null direction), eliciting a mix of bursts (black) and isolated spikes (gray). *C*: an example trace when the object moves from left to right (preferred direction), eliciting a greater number of spikes than in the null direction. *D*: changing g_T from 0.20 to 0.28 μS has little effect on the response in the null direction. *E*: the increase in the g_T current dramatically increases burst firing when the object moves in the preferred direction.

because the identity of a spike as a burst or isolated spike is only determined by the time interval separating it from the next action potential firing. It is necessary to know when the next spike occurs to classify any given spike as part of a burst or not if using the simple ISI threshold procedure that was described above. It is, at best, unclear how a sensory system would implement this.

Decoding bursts using synaptic facilitation. Previous studies have proposed that synapses with strong facilitation and/or high probability of failure would be insensitive to isolated spikes but would respond to bursts (Kepecs and Lisman 2003; Kepecs et al. 2002; Lisman 1997). These theoretical results have been confirmed in experimental studies that have shown that bursts of action potentials are indeed more reliable at eliciting plasticity in synapses (Harvey-Girard et al. 2010). However, it is not clear whether such a system would preferentially extract the burst spikes in responses to moving objects.

We tested whether a synapse with strong facilitation would be sufficient to decode directional information transmitted by a presynaptic spike train (Fig. 9*A*). The model displays different

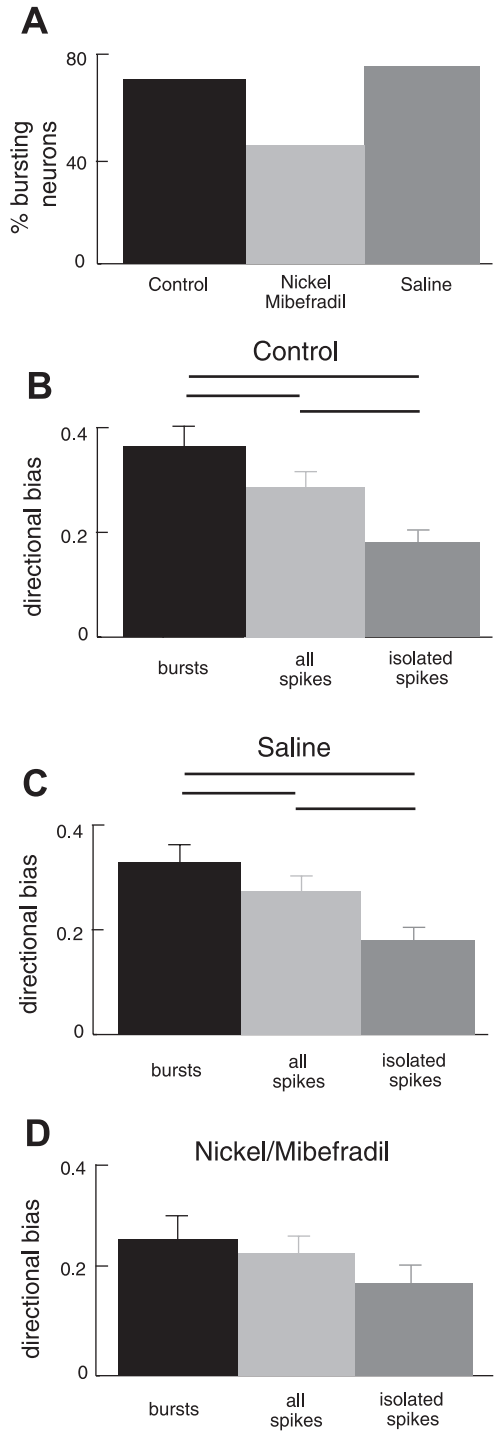

Fig. 8. Testing the model's prediction. *A*: percentage of neurons that exhibited bursting under control conditions, after injection of either $NiCl_2$ or mibefradil, and after saline injection (artificial cerebrospinal fluid, ACSF). *B–D*: DB computed from bursts, all spikes, and isolated spikes under control conditions (*B*), after saline injection (*C*), and after $NiCl_2$/mibefradil injection (*D*). Horizontal bars indicate statistical significance at the $P = 0.05$ level using a signed-rank test.

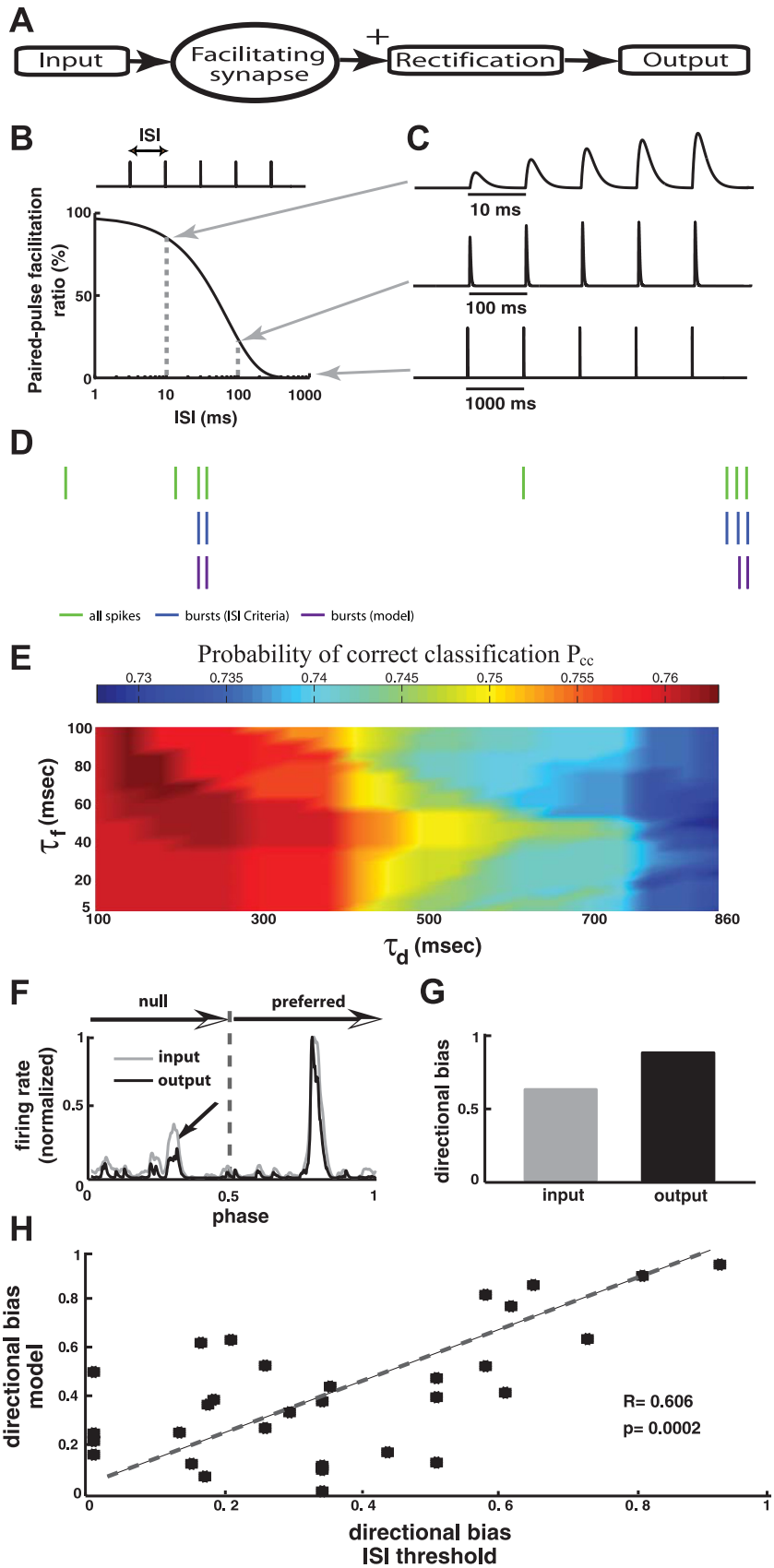

Fig. 9. Decoding information carried by bursts. *A*: schematic of our decoding model. It consists of a facilitating excitatory synapse followed by half-wave rectification. *B*: response of the model to a tetanus consisting of 5 presynaptic spikes with time interval I (*top*) quantified by the paired-pulse facilitation ratio as a function of I. *C*: model responses to tetani with I = 10, 100, and 1,000 ms. *D*: performance of the decoding model compared with performance of an ISI threshold criterion. Shown are the original spike train (green ticks), the spikes that belong to bursts according to the ISI threshold (blue ticks), and the spikes that belong to bursts according to the decoding model (purple ticks). *E*: probability of correct classification (P_{cc}) as a function of the facilitation (τ_f) and depression (τ_d) time constants. *F*: input PSTH (gray) and output PSTH (black) from the model when the input consists of the full spike train from the neuron shown in Fig. 2*A*. *G*: output DB (black) and input DB (gray) computed from the PSTHs shown in *F*. *H*: DB of bursts computed from the decoding model as a function of the DB of bursts computed from the ISI threshold criterion. There was a significant positive correlation between both quantities (R = 0.606, P = 0.0002, n = 32).

levels of facilitation in response to tetanic stimulation consisting of five presynaptic action potentials separated by an ISI *I* as *I* is systematically varied (Fig. 9*B*). The model displayed strong facilitation for $I = 10$ ms, weaker facilitation for $I = 100$ ms, and no significant facilitation for $I = 1{,}000$ ms (Fig. 9*C*, compare *top*, *middle*, and *bottom* panels). This was confirmed by plotting the paired-pulse facilitation ratio (i.e., the amplitude of the second EPSP minus the amplitude of the first EPSP normalized to the amplitude of the first EPSP) as a function of *I*: this ratio decreases monotonically to zero as a function of increasing *I* (Fig. 9*B*) and illustrates this model's ability to respond preferentially to bursts by effectively implementing a high-pass filter on the inverse interspike interval sequence.

We next tested whether this simple model could segregate bursts from isolated spikes and compared its performance to that of an ISI threshold. A representative example is shown in Fig. 9*D*: this model can effectively segregate bursts from isolated spikes. We quantified the model's performance by using signal detection theory and found that this model could give ~75% probability of correct classification for a wide range of parameters (Fig. 9*E*). We next presented experimentally measured spike trains from TS neurons to the model and computed the PSTH. Our results show that this model was indeed sensitive primarily to bursts. When the full spike train of the neuron shown in Fig. 2*A* was used as input, the output PSTH displayed a reduction of the peak response in the null direction (Fig. 9*F*, arrow) and was similar to that obtained by using only the bursts (compare Fig. 9*F*, black, with Fig. 2*A*, blue).

Consequently, the output directional bias of the model was larger than the input directional bias present in the input spike train (Fig. 9*G*). Finally, we computed the directional bias of bursts obtained with our model against that computed from bursts obtained with the ISI threshold criterion across our data set (Fig. 9*H*) and observed a significant positive correlation between both quantities ($R = 0.606$, $P = 0.0002$, $n = 32$). In conclusion, our results show that a biophysical realistic model of plasticity can reliably extract bursts from incoming spike trains. As such, the directional information carried by the bursts of TS neurons can in theory be decoded by downstream neurons.

DISCUSSION

We have shown that most direction-selective neurons in the midbrain of weakly electric fish preferentially encode the direction of movement using bursts. We found that ~70% of the neurons in our data set fired bursts of action potentials in response to moving object stimuli and that, for these neurons, bursts carried significantly greater directional information than either all spikes or isolated spikes. It is unlikely that this result is an artifact of the ISI burst threshold technique that we used to segregate bursts from isolated spikes, because qualitatively different results were obtained in nonbursting neurons. In nonbursting neurons, arbitrary divisions of spikes into bursts and isolated spikes did not result in increased direction selectivity by bursts.

To better understand these results, we built a mathematical model of directional selectivity in TS neurons that incorporated a T-type calcium conductance. This model predicted that bursts of action potentials could result from the transient deinactivation of the T-type conductance by membrane hyperpolarization and that this mechanism could preferentially elicit bursts in the preferred direction. Moreover, the model predicted that after the T-type conductance was blocked, bursts would not carry greater directional information than either all spikes or isolated spikes.

We tested this prediction experimentally by injecting calcium channel antagonists in TS. We found that TS neurons, after this injection, displayed significantly less tendency to burst. Furthermore, the directional biases of bursts, isolated spikes, and all spikes were quantitatively similar under these conditions, which was reminiscent of results obtained for nonbursting TS neurons under control conditions. These results support our model's prediction that directionally biased interactions between afferent input and T-type calcium channels mediate the enhancement of direction selectivity by burst spikes.

Finally, we have shown that a model downstream decoder, using simple biologically realistic neural circuits, can selectively extract bursts from spike trains consisting of both bursts and isolated spikes. This model decoder was shown to perform similarly to an ISI threshold. As such, our results show that downstream neurons could actually decode motion information that is carried by bursts of action potentials.

Burst and isolated spikes in direction-selective circuits. We have shown that the standard method for measuring direction selectivity, in which the firing rates elicited by each direction of movement are compared, can underestimate direction selectivity and fail to capture salient information transmitted by the neurons. Indeed, bursts were almost always more directionally selective than the full spike trains in bursting neurons, which was largely due to the fact that isolated spikes carried little or no directional information. Our results thus show that burst firing caused by T-type calcium channels can amplify this bias. However, burst firing alone will not necessarily make a neuron more directionally selective. Indeed, previous studies have shown that TS neurons receive varying degrees of input directional bias (Chacron et al. 2009), and these differences may explain why nonbursting and bursting neurons displayed similar levels of directional selectivity in their full spike trains on average. Further studies are needed to understand this.

Our results may have implications for the analysis of direction selectivity in mammalian visual cortex. Indeed, the electrosensory system has many parallels with thalamocortical pathways (Krahe and Gabbiani 2004). In particular, thalamic relay neurons within the lateral geniculate nucleus (LGN) display an intrinsic burst mechanism that is mediated by subthreshold T-type calcium channels that has been both biophysically characterized and modeled (Jahnsen and Llinas 1984; Lu et al. 1992; McCormick and Huguenard 1992; Mukherjee and Kaplan 1995; Rush and Rinzel 1994; Sherman 2001; Sherman and Guillery 2002, 2006; Smith et al. 2000). These neurons have two modes of action potential firing in vitro (Sherman 2001), and studies performed in vivo have shown that their spike trains in vivo consist of both bursts and isolate spikes in awake behaving animals (Lesica and Stanley 2004; Reinagel et al. 1999; Wolfart et al. 2005).

Although previous studies have shown that these neurons are not directionally selective (Hubel and Wiesel 1962), these studies did not consider action potential patterns such as bursts. We hypothesize that bursts of action potentials from thalamic

relay neurons in LGN carry specific directional information that is then used by postsynaptic neurons within the primary visual cortex to generate directionally biased responses. This hypothesis is supported by the fact that thalamocortical synapses display strong depression, and sustained isolated action potential firing from thalamic relay neurons activates this depression (Sherman 1996, 2001; Sherman and Guillery 2006). Nevertheless, after ~100 ms of membrane hyperpolarization, T-type calcium currents in these neurons can cause burst firing, which could amplify the postsynaptic responses to bursts (Sherman 1996, 2001; Sherman and Guillery 2006). Studies performed within the LGN are necessary to validate this hypothesis.

Furthermore, these results might also be relevant in understanding auditory processing within the inferior colliculus (IC), because it is homologous to the TS in gymnotiform weakly electric fishes. IC neurons display a form of direction selectivity, responding to either ascending or descending frequency-modulated acoustic sweeps (Fuzessery and Hall 1996; Fuzessery et al. 2006; Razak and Fuzessery 2006, 2008; Suga 1965). We hypothesize that T-type calcium channel-mediated burst firing within the IC could be used to improve the degree of response selectivity to ascending vs. descending frequency-modulated acoustic sweeps. Further studies are needed to test this hypothesis.

Removing T-type calcium channel inactivation by hyperpolarization. We have shown that a period of hyperpolarization is seen immediately before burst firing in TS neurons. Such hyperpolarization is needed to remove the inactivation of the T-type conductance, thereby leading to a burst of action potentials riding on top of the calcium spike (Llinas and Jahnsen 1982). Our previous experimental results indicated that the T-type conductance is predominantly activated in the preferred direction (Chacron and Fortune 2010). Our current results show that there is a greater membrane hyperpolarization when the object moves in the preferred direction, which in turn leads to the greater activation of the T-type calcium conductance. Where does this hyperpolarization come from? A priori, such hyperpolarization could come from inhibitory connections within the TS. However, this would be inconsistent with our previous results showing that GABAergic and glycinergic antagonists do not alter directional selectivity in TS neurons (Chacron and Fortune 2010). Alternatively, this hyperpolarization could come from a decrease in excitation. Indeed, TS neurons receive exclusively excitatory afferent input from ELL pyramidal cells (Carr and Maler 1985). We therefore hypothesize that the membrane hyperpolarization seen experimentally is caused by a decrease in the excitation coming from I-type pyramidal cells that are inhibited during the passage of the moving object in their receptive fields. We note that models in which the outputs of ON and OFF cells are spatially offset have been proposed to explain directional selectivity in the visual system (Hubel and Wiesel 1962). However, further studies are needed to validate this hypothesis in the electrosensory system and are beyond the scope of this report.

Role of active burst dynamics in generating directional selectivity. Previous studies have suggested that bursts are more likely to transmit behaviorally relevant information than isolated spikes because they can overcome synaptic unreliability in downstream neurons (Lisman 1997). Indeed, bursts of action potentials have been shown to be more reliable than isolated spikes at inducing changes in the postsynaptic neuron such as synaptic plasticity (Gall et al. 2005; Harvey-Girard et al. 2010; Lisman 1997) and can be more reliable indicators of stimulus features such as orientation in the visual system of mammals (Lisman 1997; Martinez-Conde et al. 2002). However, we are not aware of previous results showing that bursts could give rise to enhanced directional selectivity. Our results have shown that, in most TS neurons, bursts are more directionally selective than the full spike train or the isolated spike train. This supports the point of view that bursts of action potentials carry salient information. Our study has shown that an active burst mechanism based on a low-threshold calcium conductance gives rise to preferential encoding of directional information by bursts. However, there are multiple mechanisms that can give rise to burst firing in neurons (Izhikevich 2000; Krahe and Gabbiani 2004). Further studies are needed to explore whether burst dynamics that are different from the one considered presently would also give rise to the same phenomenon.

Selective burst extraction by downstream circuits. We have proposed a biologically plausible neural circuit that can selectively extract bursts. Although it is frequently assumed that bursts can be segregated from isolated spikes in the brain (Avila-Akerberg and Chacron 2011; Avila-Akerberg et al. 2010; Bastian and Nguyenkim 2001; Chacron and Bastian 2008; Doiron et al. 2007; Gabbiani et al. 1996; Kepecs and Lisman 2003; Oswald et al. 2004, 2007), biophysically plausible implementations by which such segregation can be achieved have not been widely considered. Previous reports have suggested potential circuits that could extract bursts (Lisman 1997), which were the theoretical basis for the model for burst extraction used in the present study. Our results have shown that such a model can perform similarly to the ISI criterion that has been frequently used by previous investigators. Our results therefore suggest that downstream neurons can decode directional information carried in the burst firing from TS neurons. In *A. leptorhynchus*, many neurons in the TS project to the optic tectum (OT), where some neurons have been shown to respond selectively to moving objects in a directionally biased fashion (Bastian 1982). However, the dynamics of TS-OT synapses are not known, and further studies should concentrate on whether OT neurons respond selectively to bursts from TS neurons and on determining whether TS-OT synapses display strong paired-pulse facilitation that would enable them to preferentially signal the occurrence of these bursts.

Functional relevance of independent burst and isolated spike codes. For most of the neurons in our data set, bursts were best at encoding the direction of movement, whereas isolated spikes carried little, if any, directional information. It is possible that, for these neurons, isolated spikes could code for a stimulus not related to movement, whereas bursts would code for the movement direction. For example, weakly electric fish produce communication calls called chirps during aggressive and courtship situations in which both animals move with respect to one another (Hupe and Lewis 2008; Zakon et al. 2002): recent studies have shown that TS neurons can respond to such stimuli with well-timed isolated spikes (Vonderschen and Chacron 2009). Such parallel coding is entirely consistent with an emerging general picture in which bursts and isolated spikes code for different stimulus attributes (Avila-Akerberg and Chacron 2011; Avila-Akerberg et al. 2010; Deemyad et al.

2011; Kepecs and Lisman 2003; Lesica and Stanley 2004; Marsat and Maler 2010; Marsat and Pollack 2004; Marsat et al. 2009; Oswald et al. 2004).

Conclusion. We have shown that bursts can convey information about movement direction more reliably than either the full or isolated spike trains in electrosensory midbrain neurons. As such, burst firing can be used to amplify a given directional bias. It is likely that burst firing is used to convey information about movement direction in other systems as well.

GRANTS

This research was supported by the Grass Foundation (E. S. Fortune, M. J. Chacron), National Science Foundation Grants IOS-0817918 and CMMI-0941674 (E. S. Fortune), Office of Naval Research Award N000140910531 (E. S. Fortune), and by the Canadian Institutes of Health Research, Fondes de Recherche du Québec-Nature et Technologies, Canada Foundation for Innovation, and Canada Research Chairs (M. J. Chacron).

DISCLOSURES

No conflicts of interest, financial or otherwise, are declared by the author(s).

REFERENCES

Abeles M. Quantification, smoothing, and confidence limits for single-units' histograms. *J Neurosci Methods* 5: 317–325, 1982.

Avila-Akerberg O, Chacron MJ. In vivo conditions influence the coding of stimulus features by bursts of action potentials. *J Comput Neurosci*. doi: 10.1007/s10827-011-0313-4.

Avila-Akerberg O, Krahe R, Chacron MJ. Neural heterogeneities and stimulus properties affect burst coding in vivo. *Neuroscience* 168: 300–313, 2010.

Bastian J. Vision and electroreception. Integration of sensory information in the optic tectum of the weakly electric fish *Apteronotus albifrons*. *J Comp Physiol A* 147: 287–297, 1982.

Bastian J, Chacron MJ, Maler L. Receptive field organization determines pyramidal cell stimulus-encoding capability and spatial stimulus selectivity. *J Neurosci* 22: 4577–4590, 2002.

Bastian J, Nguyenkim J. Dendritic Modulation of Burst-like firing in sensory neurons. *J Neurophysiol* 85: 10–22, 2001.

Bloodgood BL, Sabatini BL. Nonlinear regulation of unitary synaptic signals by CaV(2.3) voltage-sensitive calcium channels located in dendritic spines. *Neuron* 53: 249–260, 2007.

Borst A. Correlation versus gradient type motion detectors: the pros and cons. *Philos Trans R Soc Lond B Biol Sci* 362: 369–374, 2007.

Borst A, Egelhaaf M. Direction selectivity of blowfly motion-sensitive neurons is computed in a two-stage process. *Proc Natl Acad Sci USA* 87: 9363–9367, 1990.

Borst A, Egelhaaf M. Principles of visual motion detection. *Trends Neurosci* 12: 297–306, 1989.

Carver S, Roth E, Cowan NJ, Fortune ES. Synaptic plasticity can produce and enhance direction selectivity. *PLoS Comput Biol* 4: e32, 2008.

Chacron MJ. Nonlinear information processing in a model sensory system. *J Neurophysiol* 95: 2933–2946, 2006.

Chacron MJ, Bastian J. Population coding by electrosensory neurons. *J Neurophysiol* 99: 1825–1835, 2008.

Chacron MJ, Doiron B, Maler L, Longtin A, Bastian J. Non-classical receptive field mediates switch in a sensory neuron's frequency tuning. *Nature* 423: 77–81, 2003.

Chacron MJ, Fortune ES. Subthreshold membrane conductances enhance directional selectivity in vertebrate sensory neurons. *J Neurophysiol* 104: 449–462, 2010.

Chacron MJ, Lindner B, Longtin A. Threshold fatigue and information transfer. *J Comput Neurosci* 23: 301–311, 2007.

Chacron MJ, Longtin A, Maler L. Delayed excitatory and inhibitory feedback shape neural information transmission. *Phys Rev E Stat Nonlin Soft Matter Phys* 72: 051917, 2005a.

Chacron MJ, Longtin A, Maler L. Efficient computation via sparse coding in electrosensory neural networks. *Curr Opin Neurobiol*. doi:10.1016/j.conb.2011.05.016.

Chacron MJ, Longtin A, Maler L. Simple models of bursting and non-bursting electroreceptors. *Neurocomputing* 38: 129–139, 2001.

Chacron MJ, Longtin A, Maler L. To burst or not to burst? *J Comput Neurosci* 17: 127–136, 2004.

Chacron MJ, Maler L, Bastian J. Feedback and feedforward control of frequency tuning to naturalistic stimuli. *J Neurosci* 25: 5521–5532, 2005b.

Chacron MJ, Toporikova N, Fortune ES. Differences in the time course of short-term depression across receptive fields are correlated with directional selectivity in electrosensory neurons. *J Neurophysiol* 102: 3270–3279, 2009.

Chance FS, Nelson SB, Abbott LF. Synaptic depression and the temporal response characteristics of V1 cells. *J Neurosci* 18: 4785–4799, 1998.

Cowan NJ, Fortune ES. The critical role of locomotion mechanics in decoding sensory systems. *J Neurosci* 27: 1123–1128, 2007.

Dayan P, Abbott LF. *Theoretical Neuroscience: Computational and Mathematical Modeling of Neural Systems*. Cambridge, MA: MIT Press, 2001.

DeBusk BC, DeBruyn EJ, Snider RK, Kabara JF, Bonds AB. Stimulus-dependent modulation of spike burst length in cat striate cortical cells. *J Neurophysiol* 78: 199–213, 1997.

Deemyad T, Maler L, Chacron MJ. Inhibition of SK and M channel mediated currents by 5-HT enables parallel processing by bursts and isolated spikes. *J Neurophysiol* 105: 1276–1294, 2011.

Derrington AM, Allen HA, Delicato LS. Visual mechanisms of motion analysis and motion perception. *Annu Rev Psychol* 55: 181–205, 2004.

Destexhe A, Rudolph M, Pare D. The high-conductance state of neocortical neurons in vivo. *Nat Rev Neurosci* 4: 739–751, 2003.

Doiron B, Noonan L, Lemon N, Turner RW. Persistent Na^+ current modifies burst discharge by regulating conditional backpropagation of dendritic spikes. *J Neurophysiol* 89: 324–337, 2003.

Doiron B, Oswald AM, Maler L. Interval coding II. Dendrite-dependent mechanisms. *J Neurophysiol* 97: 2744–2757, 2007.

Euler T, Detwiler PB, Denk W. Directionally selective calcium signals in dendrites of starburst amacrine cells. *Nature* 418: 845–852, 2002.

Eyherabide HG, Rokem A, Herz AV, Samengo I. Burst firing is a neural code in an insect auditory system. *Front Comput Neurosci* 2: 3, 2008.

Fortune ES, Chacron MJ. Physiology of tuberous electrosensory systems. In: *Encyclopedia of Fish Physiology: From Genome to Environment*, edited by Farrell AP. San Diego, CA: Academic, 2011, p. 366–374.

Frank K, Becker MC. Microelectrodes for recording and stimulation. In: *Physical Techniques in Biological Research, Part A*, edited by Nastuk L. New York: Academic, 1964, p. 22–87.

Fuzessery ZM, Hall JC. Role of GABA in shaping frequency tuning and creating FM sweep selectivity in the inferior colliculus. *J Neurophysiol* 76: 1059–1073, 1996.

Fuzessery ZM, Richardson MD, Coburn MS. Neural mechanisms underlying selectivity for the rate and direction of frequency-modulated sweeps in the inferior colliculus of the pallid bat. *J Neurophysiol* 96: 1320–1336, 2006.

Gabbiani F, Koch C. Principles of spike train analysis. In: *Methods in Neuronal Modeling: From Ions to Networks*, edited by Koch C and Segev I. Cambridge, MA: MIT Press, 1998, p. 313–360.

Gabbiani F, Metzner W, Wessel R, Koch C. From stimulus encoding to feature extraction in weakly electric fish. *Nature* 384: 564–567, 1996.

Gall D, Prestori F, Sola E, D'Errico A, Roussel C, Forti L, Rossi P, D'Angelo E. Intracellular calcium regulation by burst discharge determines bidirectional long-term synaptic plasticity at the cerebellum input stage. *J Neurosci* 25: 4813–4822, 2005.

Gaudry KS, Reinagel P. Information measure for analyzing specific spiking patterns and applications to LGN bursts. *Network* 19: 69–94, 2008.

Gray C, Singer W. Stimulus-specific neuronal oscillations in orientation columns of cat visual cortex. *Proc Natl Acad Sci USA* 86: 1698–1702, 1989.

Green D, Swets J. *Signal Detection Theory and Psychophysics*. New York: Wiley, 1966.

Haag J, Denk W, Borst A. Fly motion vision is based on Reichardt detectors regardless of the signal-to-noise ratio. *Proc Natl Acad Sci USA* 101: 16333–16338, 2004.

Harvey-Girard E, Lewis JE, Maler L. Burst-induced anti-Hebbian depression acts through short-term synaptic dynamics to cancel redundant sensory signals. *J Neurosci* 30: 6152–6169, 2010.

Hitschfeld ÉM, Stamper SA, Vonderschen K, Fortune ES, Chacron MJ. Effects of restraint and immobilization on electrosensory behaviors of weakly electric fish. *ILAR J* 50: 361–372, 2009.

Hock HS, Schoner G, Gilroy L. A counterchange mechanism for the perception of motion. *Acta Psychol (Amst)* 132: 1–21, 2009.

Hubel DH, Wiesel TN. Receptive fields, binocular interaction and functional architecture in the cat's visual cortex. *J Physiol* 160: 106–154, 1962.

Hupe GJ, Lewis JE. Electrocommunication signals in free swimming brown ghost knifefish, *Apteronotus leptorhynchus*. *J Exp Biol* 211: 1657–1667, 2008.

Izhikevich EM. Neural excitability, spiking and bursting. *Int J Bifurcation Chaos* 10: 1171–1269, 2000.

Jagadeesh B, Wheat HS, Kontsevich LL, Tyler CW, Ferster D. Direction selectivity of synaptic potentials in simple cells of the cat visual cortex. *J Neurophysiol* 78: 2772–2789, 1997.

Jahnsen H, Llinas R. Electrophysiological properties of guinea-pig thalamic neurones: an in vitro study. *J Physiol* 349: 205–226, 1984.

Kepecs A, Lisman J. Information encoding and computation with spikes and bursts. *Network* 14: 103–118, 2003.

Kepecs A, Wang XJ, Lisman J. Bursting neurons signal input slope. *J Neurosci* 22: 9053–9062, 2002.

Kloeden PE, Platen E. *Numerical Solutions of Stochastic Differential Equations*. Berlin: Springer, 1999.

Krahe R, Bastian J, Chacron MJ. Temporal processing across multiple topographic maps in the electrosensory system. *J Neurophysiol* 100: 852–867, 2008.

Krahe R, Gabbiani F. Burst Firing in Sensory Systems. *Nat Rev Neurosci* 5: 13–23, 2004.

Lesica NA, Stanley GB. Encoding of natural scene movies by tonic and burst spikes in the lateral geniculate nucleus. *J Neurosci* 24: 10731–10740, 2004.

Lewis JE, Maler L. Dynamics of electrosensory feedback: short-term plasticity and inhibition in a parallel fiber pathway. *J Neurophysiol* 88: 1695–1706, 2002.

Lewis JE, Maler L. Synaptic dynamics on different time scales in a parallel fiber feedback pathway of the weakly electric fish. *J Neurophysiol* 91: 1064–1070, 2004.

Lindner B, Gangloff D, Longtin A, Lewis JE. Broadband coding with dynamic synapses. *J Neurosci* 29: 2076–2087, 2009.

Lisman JE. Bursts as a unit of neural information: making unreliable synapses reliable. *Trends Neurosci* 20: 38–43, 1997.

Llinas RL, Jahnsen H. Electrophysiology of mammalian thalamic neurons in vitro. *Nature* 297: 406–408, 1982.

Lu SM, Guido W, Sherman SM. Effects of membrane voltage on receptive field properties of lateral geniculate neurons in the cat: contributions of the low-threshold Ca^{2+} conductance. *J Neurophysiol* 68: 2185–2198, 1992.

Macleod K, Laurent G. Distinct mechanisms for synchronization and temporal patterning of odor-encoding neural assemblies. *Science* 274: 976–979, 1996.

Maex R, Orban GA. Subtraction inhibition combined with a spiking threshold accounts for cortical direction selectivity. *Proc Natl Acad Sci USA* 88: 3549–3553, 1991.

Maler L. Receptive field organization across multiple electrosensory maps. I. Columnar organization and estimation of receptive field size. *J Comp Neurol* 516: 376–393, 2009.

Manwani A, Koch C. Detecting and estimating signals in noisy cable structure. I: neuronal noise sources. *Neural Comput* 11: 1797–1829, 1999.

Marsat G, Maler L. Neural heterogeneity and efficient population codes for communication signals. *J Neurophysiol* 104: 2543–2555, 2010.

Marsat G, Pollack GS. Differential temporal coding of rhythmically diverse acoustic signals by a single interneuron. *J Neurophysiol* 92: 939–948, 2004.

Marsat G, Pollack GS. The structure and size of sensory bursts encode stimulus information but only size affects behavior. *J Comp Physiol A* 196: 315–320, 2010.

Marsat G, Proville RD, Maler L. Transient signals trigger synchronous bursts in an identified population of neurons. *J Neurophysiol* 102: 714–723, 2009.

Martinez-Conde S, Macknik SL, Hubel DH. The function of bursts of spikes during visual fixation in the awake primate lateral geniculate nucleus and primary visual cortex. *Proc Natl Acad Sci USA* 99: 13920–13925, 2002.

McCormick DA, Huguenard JR. A model of the electrophysiological properties of thalamocortical relay neurons. *J Neurophysiol* 68: 1384–1400, 1992.

Mehrke G, Zong XG, Flockerzi V, Hofmann F. The Ca^{++}-channel blocker Ro 40–5967 blocks differently T-type and L-type Ca^{++} channels. *J Pharmacol Exp Ther* 271: 1483–1488, 1994.

Mukherjee P, Kaplan E. Dynamics of neurons in the cat lateral geniculate nucleus: in vivo electrophysiology and computational modeling. *J Neurophysiol* 74: 1222–1243, 1995.

Nelson ME, MacIver MA. Prey capture in the weakly electric fish *Apteronotus albifrons*: sensory acquisition strategies and electrosensory consequences. *J Exp Biol* 202: 1195–1203, 1999.

Oswald AM, Doiron B, Maler Interval coding L. I. Burst interspike intervals as indicators of stimulus intensity. *J Neurophysiol* 97: 2731–2743, 2007.

Oswald AMM, Chacron MJ, Doiron B, Bastian J, Maler L. Parallel processing of sensory input by bursts and isolated spikes. *J Neurosci* 24: 4351–4362, 2004.

Priebe NJ, Ferster D. Inhibition, spike threshold, and stimulus selectivity in primary visual cortex. *Neuron* 57: 482–497, 2008.

Priebe NJ, Mechler F, Carandini M, Ferster D. The contribution of spike threshold to the dichotomy of cortical simple and complex cells. *Nat Neurosci* 7: 1113–1122, 2004.

Ramcharitar JU, Tan EW, Fortune ES. Effects of global electrosensory signals on motion processing in the midbrain of Eigenmannia. *J Comp Physiol A* 191: 865–872, 2005.

Ramcharitar JU, Tan EW, Fortune ES. Global electrosensory oscillations enhance directional responses of midbrain neurons in eigenmannia. *J Neurophysiol* 96: 2319–2326, 2006.

Razak KA, Fuzessery ZM. Facilitatory mechanisms underlying selectivity for the direction and rate of frequency modulated sweeps in the auditory cortex. *J Neurosci* 28: 9806–9816, 2008.

Razak KA, Fuzessery ZM. Neural mechanisms underlying selectivity for the rate and direction of frequency-modulated sweeps in the auditory cortex of the pallid bat. *J Neurophysiol* 96: 1303–1319, 2006.

Reichardt W. Evaluation of optical motion information by movement detectors. *J Comp Physiol A* 161: 533–547, 1987.

Reichardt W, Wenking H. Optical detection and fixation of objects by fixed flying flies. *Naturwissenschaften* 56: 424–425, 1969.

Reinagel P, Godwin D, Sherman SM, Koch C. Encoding of visual information by LGN bursts. *J Neurophysiol* 81: 2558–2569, 1999.

Rieke F, Warland D, de Ruyter van Steveninck RR, Bialek W. *Spikes: Exploring the Neural Code*. Cambridge, MA: MIT Press, 1996.

Rose GJ, Fortune ES. New techniques for making whole-cell recordings from CNS neurons in vivo. *Neurosci Res* 26: 89–94, 1996.

Rush ME, Rinzel J. Analysis of bursting in a thalamic neuron model. *Biol Cybern* 71: 281–291, 1994.

Samengo I, Montemurro MA. Conversion of phase information into a spike-count code by bursting neurons. *PLoS One* 5: e9669, 2010.

Saunders J, Bastian J. The physiology and morphology of two classes of electrosensory neurons in the weakly electric fish *Apteronotus leptorhynchus*. *J Comp Physiol A* 154: 199–209, 1984.

Savard M, Krahe R, Chacron MJ. Neural heterogeneities influence envelope and temporal coding at the sensory periphery. *Neuroscience* 172: 270–284, 2011.

Sherman SM. Dual response modes in lateral geniculate neurons: mechanisms and functions. *Vis Neurosci* 13: 205–213, 1996.

Sherman SM. Tonic and burst firing: dual modes of thalamocortical relay. *Trends Neurosci* 24: 122–126, 2001.

Sherman SM, Guillery RW. *Exploring the Thalamus and its Role in Cortical Function*. Cambridge, MA: MIT Press, 2006.

Sherman SM, Guillery RW. The role of the thalamus in the flow of information to the cortex. *Philos Trans R Soc Lond B Biol Sci* 357: 1695–1708, 2002.

Sillito AM, Jones HE, Gerstein GL, West DC. Feature-linked synchronization of thalamic relay cell firing induced by feedback from the visual cortex. *Nature* 369: 479–482, 1994.

Smith GD, Cox CL, Sherman SM, Rinzel J. Fourier analysis of sinusoidally driven thalamocortical relay neurons and a minimal integrate-and fire-or-burst model. *J Neurophysiol* 83: 588–610, 2000.

Srinivasan MV, Poteser M, Kral K. Motion detection in insect orientation and navigation. *Vision Res* 39: 2749–2766, 1999.

Suga N. Analysis of frequency-modulated sounds by auditory neurones of echo-locating bats. *J Physiol* 179: 26–53, 1965.

Toporikova N, Chacron MJ. Dendritic SK channels gate information processing in vivo by regulating an intrinsic bursting mechanism seen in vitro. *J Neurophysiol* 102: 2273–2287, 2009.

Turner RW, Maler L, Burrows M. Electroreception and electrocommunication. *J Exp Biol* 202: 1167–1458, 1999.

Turner RW, Maler L, Deerinck T, Levinson SR, Ellisman MH. TTX-sensitive dendritic sodium channels underlie oscillatory discharge in a vertebrate sensory neuron. *J Neurosci* 14: 6453–6471, 1994.

Vonderschen K, Chacron MJ. Sparse coding of natural communication signals in midbrain neurons. *BMC Neurosci* 10: O3, 2009.

Wolfart J, Debay D, Le Masson G, Destexhe A, Bal T. Synaptic background activity controls spike transfer from thalamus to cortex. *Nat Neurosci* 8: 1760–1767, 2005.

Zakon HH, Oestreich J, Tallarovic S, Triefenbach F. EOD modulations of brown ghost electric fish: JARs, chirps, rises, and dips. *J Physiol (Paris)* 96: 451–458, 2002.